MODELING ELECTRICAL ACTIVITY IN THE HUMAN HEART

by

Mary Catherine MacLachlan

Thesis

submitted in partial fulfillment of

the requirements of the Degree of

Bachelor of Science with Honours in

Mathematics and Statistics.

Acadia University

March 2001

This thesis by Mary C. MacLachlan

is accepted in its present form by the

Department of Mathematics and Statistics

as satisfying the thesis requirements for the Degree of

Bachelor of Science with Honours.

Approved by the Thesis Supervisor

Dr. R. Spiteri   Date

Approved by the Head of the Department

Dr. T. Archibald   Date

Approved by the Honours Committee

Date

I, Mary C. MacLachlan, hereby grant permission to the University Librarian at Acadia University to provide copies of the thesis, on request, on a non-profit basis.

Signature of Author

Signature of Supervisor

Date

Acknowledgements

I would like to thank Dr. Raymond Spiteri for supervising this project and for all his help and patience. I would also like to thank Acadia University, the Department of Mathematics and Statistics, and Dr. Spiteri for the funding which made this research possible. To the Department of Mathematics and Statistics, Dr. Tom Archibald, and Dr. Spiteri I extend my many thanks for all the great opportunities you have provided. Thanks to Colin Macdonald for all the help with LaTeX. Finally, thanks to my family, Dad, Mom, Jean, and Diane, for all their love and support.

Table of Contents

Abstract

The electrical activity responsible for every beat of the heart can be modeled mathematically. A complete mathematical picture of the electrical activity includes modeling the ionic movement which generates it as well as its propagation in cardiac muscle, specifically ventricular muscle. The ionic activity is modeled using ordinary differential equations (ODEs) as given by the Luo-Rudy Phase I model, whereas the spread of the electrical impulses is described by a partial differential equation (PDE). Coupling the ODEs with the PDE results in a physiologically accurate mathematical representation of an important process.

The equations were solved in an annular region (internal radius 4cm, external radius 5cm) representing a cross-section through the ventricle. The model incorporated the shape of the muscle fibers as well as their anisotropic conductivity. Matlab's PDE Toolbox was used to solve the equations to give a simulation for the propagation of the electrical activity in ventricular muscle.

Chapter 1

Introduction

The electrical activity of the heart can be modeled mathematically and it is the goal of this thesis to describe a physiologically accurate mathematical model for the propagation of this activity in ventricular muscle through numerical simulation. In order to understand the mathematical model, a brief introduction to the underlying biology is necessary. This model for the propagation of electrical activity in ventricular muscle involves the Luo-Rudy model for the cardiac action potential so we begin our discussion with background information at the molecular level of the cell. The structure of the cell membrane is discussed, followed by the ionic activity across it and the impact of this on cardiac muscle cells. The means by which the electrical activity spreads through the heart is also presented, followed by the derivation of the model in terms of the physiology it represents.

1.1 The Cell Membrane

Separating the cell from its environment is a structure known as the *cell membrane* or plasma membrane. It is a *phospholipid bilayer*, a double layer of phospholipid molecules arranged such that the hydrophilic (water-loving) phosphate heads of the molecules are pointing outward, while the hydrophobic (water-fearing) lipid tails are pointing inward [2]. Embedded in this bilayer are *integral proteins* which span the membrane, creating channels for passage through the membrane. Because of their function, these proteins are also referred to as *transport proteins.* Figure 1.1 shows a cross-section of the cell membrane and its transport proteins. The cell membrane

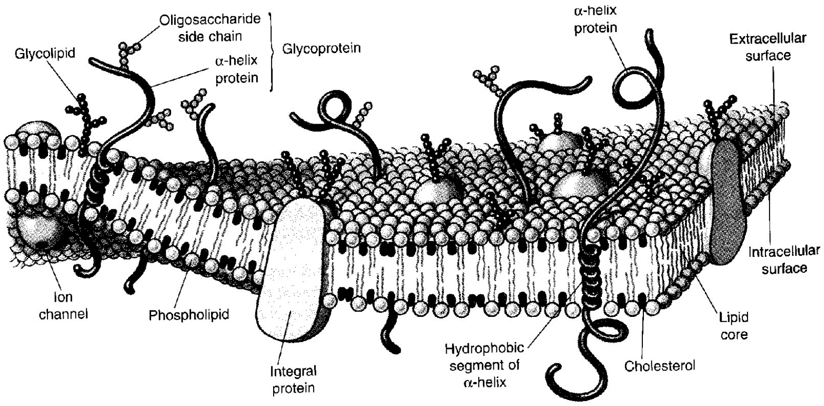

Figure 1.1: Cross-section of cell membrane. (Source: [10])

is *semipermeable*, that is, it allows the passage of certain materials while inhibiting that of others. This selectivity is dependent on the discriminating nature of the lipid membrane as well as the specificity of the transport proteins in the membrane [2].

Passage across the cell membrane is accomplished in one of two ways: through the lipid bilayer itself (i.e., between lipid molecules) or through proteins. The type of transport is dictated by the type of molecule. For example, small lipid-soluble molecules may move through the membrane by passing between the phospholipid molecules because they can dissolve in the lipid bilayer. Ions and other polar substances that are not lipid-soluble rely on the transport proteins for movement across the membrane. This is known as *facilitated diffusion.* Transport proteins can provide merely a channel for passage or they can bind a molecule and change their conformation (structure) to move the molecule from one side of the membrane to the other. Both these processes are passive; that is, they require no energy expenditure. Concentration and electrical gradients dictate the movement of the molecules. Some transport proteins, however, are membrane pumps which expend energy (in the form of ATP[1]) to move substances against their gradients. The proteins are specific to the substance they will transport. The movement of interest here is the passive movement of sodium, potassium, and calcium ions. These ions move through water-filled proteins channels, down their gradients. The movement of these ions is of concern for the currents and the voltage differences their movement generates.

1.2 The Action Potential

Across the cell membrane there exists a difference in electrical potential, a voltage difference where the inside of the cell is negatively charged with respect to the outside. This voltage difference is characteristic of all cells, and is known as the cell's *resting potential*. A particular group of cells, *excitable cells*, generate reversals in the membrane potential when stimulated; these changes are called *action potentials*. In order for an action potential to occur, a stimulus current large enough to raise the membrane's potential above a threshold value must be applied. Once the potential exceeds the threshold, a complete charge reversal takes place as the cell depolarizes to a positive voltage and then repolarizes back to its resting potential. When this happens, the cell is said to have *fired*. There is no partial firing of excitable cells. Action potentials are *all-or-nothing* events that occur each time the threshold voltage is exceeded [10]. Changes in the membrane potential are the result of changes in the membrane's permeability to particular ions; this is accomplished via *voltage gated channels*, protein channels that open and close in response to changes in the membrane potential. A change in the membrane's permeability to a particular ion is a change in that ion's *conductance*. Ions carry a charge, so their entrance and exit of the cell has an effect on the charge distribution across the membrane, and thus on the membrane potential.

[1]Adenosine Triphosphate

The excitable cells of particular interest for this study are *myocardial cells*, the muscle cells of the heart. The action potentials which these cells undergo coordinate the heart's contraction. A typical cardiac action potential is shown in Figure 1.2. The ions of importance in cardiac action potentials are sodium, potassium, and calcium.

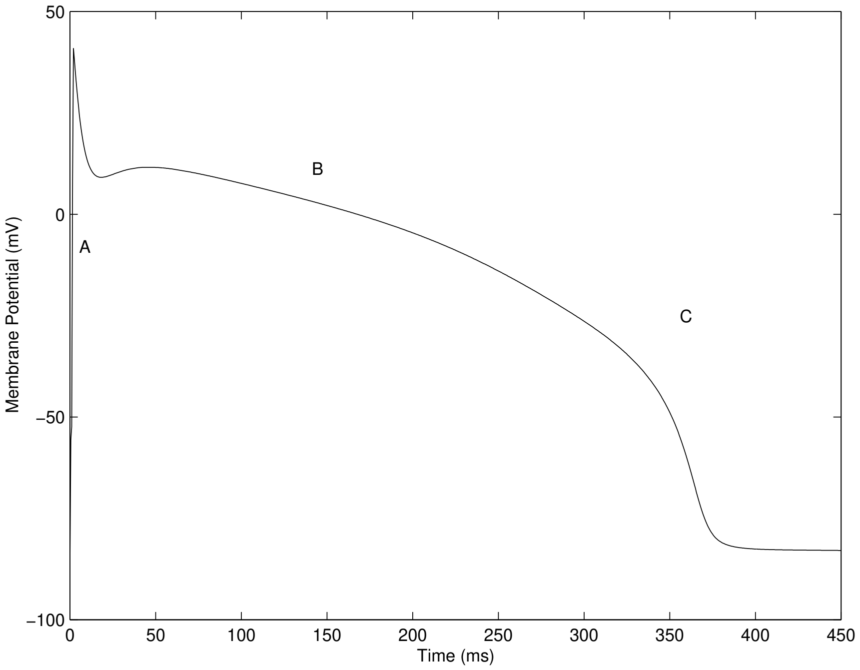

Figure 1.2: Typical cardiac action potential.

The three phases of the cardiac action potential are marked by changes in the conductance of one or more of these ions. The three phases are labelled in Figure 1.2. The first phase, depolarization (A) is the result of a large and rapid increase in sodium conductance so that it exceeds the potassium conductance. As the action potential reaches it peak, sodium conductance declines. The plateau phase (B) is next and is prolonged in cardiac muscle cells as the result of high calcium conductance and a delay in the increase of potassium conductance. The rapid repolarization (C) marks the end of the plateau phase. This is the result of a fall in calcium conductance and an increase in potassium conductance.

The action potentials of cardiac muscle differ from those of skeletal muscle in the long length of the plateau phase. This produces a long action potential and consequently a long contraction that ensure efficient pumping of blood. The plateau keeps the membrane in a refractory state while the muscle contracts. This means that no stimulus, however large, can cause an action potential to occur during this time.

1.3 The Heart

The focus of this thesis lies with the propagation of electrical activity in ventricular muscle. However, contraction of the ventricles is the last of the sequence of events in the cardiac cycle. Thus, it is necessary to see what activity, specifically electrical, precedes the ventricular action potentials and thus ventricular contraction.

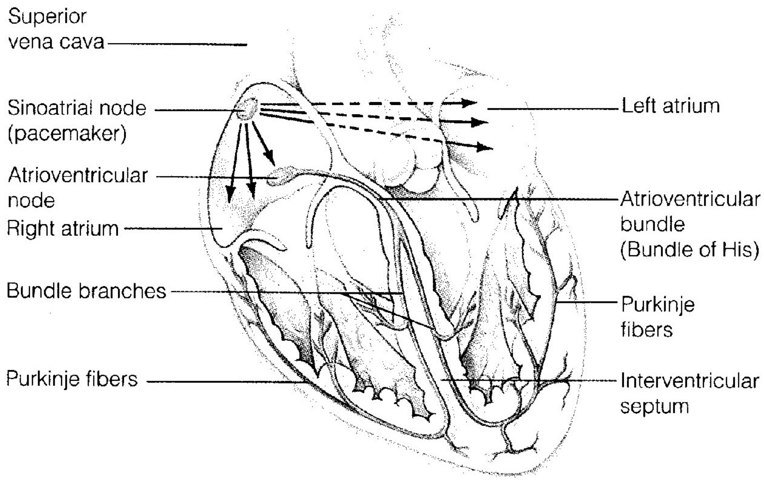

Figure 1.3: Conduction pathway in the heart. (Source: [8])

The heart has an extensive network of nervous tissue that creates a conduction pathway throughout the heart connecting the atria and the ventricles. This conduction pathway is shown in Figure 1.3. The *sinoatrial node*, located in the right atrium, is the heart's pacemaker; it sets the rate at which the heart contracts. This specialized piece of tissue can initiate its own impulses but is also innervated (supplied with nerves) by the autonomic nervous system. Impulses from the sinoatrial node spread throughout the atria because of the electrical coupling of muscle cells by means of *intercalated disks*[2] [10]. From the sinoatrial node, the impulse is carried by neuromuscular tissue to the atrioventricular node. The impulse is briefly delayed here to insure that atrial contraction is complete before ventricular contraction begins. This allows time for the ventricles to fill completely and thus is important for the efficient pumping of blood. The *Bundle of His* extends from the atrioventricular node and branches out into the right and left ventricular walls with further branching in the muscle called *Purkinje fibres*. The Bundle of His and the Purkinje fibres conduct the impulses rapidly to all areas of the the ventricle enabling all the muscle fibres to contract together as a unit, a *synctium*.

Now that we have traced the electrical activity to the ventricular muscle, we will look at a mathematical model describing the propagation of the electrical impulses in this region.

1.4 The Model

The mathematical model used to describe the propagation of electrical impulses in ventricular muscle is composed of a set of eight ordinary differential equations proposed by Luo and Rudy [7] describing the ionic activity in the muscle cells, coupled with a parabolic partial differential equation incorporating the conductivities and shape of the muscle fibres. We begin with the Luo-Rudy model.

1.4.1 The Luo-Rudy Phase I Model for the Cardiac Action Potential

The Luo-Rudy Phase I model for the cardiac action potential is one of the most physiologically correct models of its type, accounting for what are believed to be the most important ionic currents responsible for cardiac action potentials. It is surpassed

[2] regions between adjacent muscles cells which have low areas of resistance (gap junctions)

only by the Luo-Rudy Phase II model which allows for varying ionic concentrations and includes the contribution of pump currents. Voltage-gated channels control the conductance of sodium, potassium, and calcium ions in cardiac muscle cells. The Luo-Rudy model describes the operation of these channels with ordinary differential equations that are Hodgkin-Huxley type gating equations specific to cardiac cells. The Luo-Rudy model describes the resulting ionic currents as products of channel conductance and the difference between membrane potential and the reversal potential for a particular ionic species. For an ionic species s, the current I_s is described as follows:

$$I_s = G_s \cdot (V_m - E_s), \tag{1.1}$$

where G_s is the channel conductance for the ionic species, V_m is the membrane potential, and E_s is the reversal potential for the species as calculated by the Nernst equation[3]. The conductance of the channel changes with changes in the membrane potential, hence the name *voltage-gated channels*. The Luo-Rudy model describes it as a function of the maximum channel conductance and activation and inactivation parameters:

$$G_s = \bar{G} \times [\text{activation/inactivation parameter(s)}], \tag{1.2}$$

where $\bar{G}_s$ is the maximum conductance of channel s.

These activation/inactivation parameters control the opening and closing of the channel and thus the amount of ions crossing the cell membrane. The activity of these parameters y is described mathematically by ordinary differential equations of

[3]The Nernst equation for the reversal potential of ionic species s is

$$E_s = \frac{RT}{z_s F} \ln \frac{[s]_e}{[s]_i},$$

where R is the gas constant, T is temperature, z_s is the valence of ion s, F is Faraday's constant, $[s]_e$ is the extracellular concentration of s, and $[s]_i$ is the intracellular concentration of s.

the form:

$$\frac{dy}{dt} = \frac{y_\infty - y}{\tau_y}, \tag{1.3}$$

where y_∞ is the steady-state value of the gate's activation/inactivation parameter, and τ_y is the time constant of the gate. Both y_∞ and τ_y are functions of rate parameters α_y and β_y, both of which are voltage dependent:

$$y_\infty = \frac{\alpha_y}{\alpha_y + \beta_y}, \tag{1.4}$$

$$\tau_y = \frac{1}{\alpha_y + \beta_y}. \tag{1.5}$$

There are six ionic currents in the Luo-Rudy model: a fast sodium current I_{Na}; a slow inward calcium current I_{si}; a time-dependent potassium current I_K; a time-independent potassium current I_{K1}; a plateau potassium current I_{K_p}; and a background potassium current I_b. Of these six, three are directly dependent on gating parameters. There are six gating parameters in total, denoted m, h, j, d, f, X. Parameters m, h, and j are for the fast sodium current, parameters d and f are for the slow inward calcium current, and parameter X is for the time-dependent potassium current. Each gating parameter is described by an ODE. These six ODEs for gating parameters are coupled with an ODE for the calcium concentration in the cell and an ODE for the membrane voltage, to make eight ODEs in total. The calcium concentration is given by,

$$\frac{d([Ca]_i)}{dt} = -10^{-4} I_{si} + 0.07(10^{-4} - [Ca]_i), \tag{1.6}$$

where $[Ca]_i$ is the intracellular calcium concentration and I_{si} is the slow inward calcium current. The membrane voltage is the result of the total transmembrane current. An electrical schematic of the membrane is shown in Figure 1.4.

The three contributing currents are I_{ion}, the sum of the six ionic currents previ-

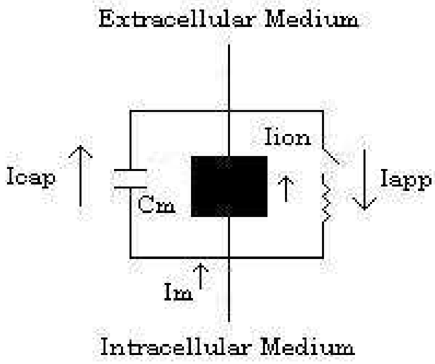

Figure 1.4: Circuit representation of the cell membrane. (Source: [1])

ously mentioned, I_{app}, the stimulus current which triggers the action potential, and I_{cap}, the capacitative current. This capacitative current is due to the separation of charges by the membrane. The membrane is impermeable to ions so it acts as an insulator, or dielectric, separating charged ions. When a voltage is applied across the membrane, the negative ions will gather close to the membrane on the positive side (extracellular side) and the positive ions will gather near the membrane on the negative (intracellular) side [10]. The membrane is thin enough so that the ions can interact electrostatically across it to produce the capacitative current,

$$I_{cap} = C_m \frac{dV_m}{dt}, \tag{1.7}$$

where C_m is the membrane capacitance. Using the circuit in Figure 1.4 and Kirchhoff's Law, the total transmembrane current I_m is given by the equation,

$$I_m = I_{cap} + I_{ion} - I_{app}. \tag{1.8}$$

Substituting for I_{cap} in (1.8) and solving for $\frac{dV_m}{dt}$ gives the ODE for membrane voltage,

$$\frac{dV_m}{dt} = -\frac{1}{C_m} \times (I_{ion} - I_{app}), \tag{1.9}$$

where C_m is the membrane capacitance, I_{ion} is the sum of the ionic currents, and I_{app} is the stimulus current.

The currents I_{ion} and I_{app}, as well as the membrane capacitance C_m are per unit area of membrane surface. Therefore, multiplying by χ, the membrane surface area per unit volume of tissue, gives the currents and capacitance per unit volume, i_{ion}, i_{app}, and c_m, respectively, and (1.9) becomes

$$\frac{dV_m}{dt} = -\frac{1}{\chi c_m} \times (i_{ion} - i_{app}). \tag{1.10}$$

The following is the complete Luo-Rudy Model with all the parameters.

1.4.2 Luo-Rudy Equations

Inward currents

Fast sodium current

$$I_{\mathrm{Na}} = \overline{G}_{\mathrm{Na}} \cdot m^3 \cdot h \cdot j \cdot (V - E_{\mathrm{Na}}) \tag{1.11}$$

Activation gate, m

$$\frac{dm}{dt} = \alpha_m(1-m) - \beta_m m \tag{1.12a}$$

$$\alpha_m = \frac{0.32(V+47.13)}{1-e^{-0.1(V+47.13)}} \tag{1.12b}$$

$$\beta_m = 0.08e^{-V/11} \tag{1.12c}$$

Fast inactivation gate, h

$$\frac{dh}{dt} = \alpha_h(1-h) - \beta_h h \tag{1.13a}$$

$$\alpha_h = \begin{cases} 0.135e^{(V+80)/-6.8} & V < -40\text{mV} \\ 0 & V \geq -40\text{mV} \end{cases} \tag{1.13b}$$

$$\beta_h = \begin{cases} 3.56e^{0.079V} + 3.1 \cdot 10^5 e^{0.35V} & V < -40\text{mV} \\ \dfrac{1}{0.13(1+e^{(V+10.66)/-11.1})} & V \geq -40\text{mV} \end{cases} \tag{1.13c}$$

Slow inactivation gate, j

$$\frac{dj}{dt} = \alpha_j(1-j) - \beta_j j \tag{1.14a}$$

$$\alpha_j = \begin{cases} \dfrac{-1.2714 \cdot 10^5 e^{0.2444V} - 3.474 \cdot 10^{-5} e^{-0.04391V} \cdot (V+37.78)}{1+e^{0.311(V+79.23)}} & V < -40\text{mV} \\ 0 & V \geq -40\text{mV} \end{cases} \tag{1.14b}$$

$$\beta_j = \begin{cases} \dfrac{0.1212e^{-0.01052V}}{1+e^{-0.1378(V+40.14)}} & V < -40\text{mV} \\ \dfrac{0.3e^{-2.535\cdot 10^{-7}V}}{1+e^{-0.1(V+32)}} & V \geq -40\text{mV} \end{cases} \tag{1.14c}$$

Slow inward current

$$I_{\text{si}} = \overline{G}_{\text{si}} \cdot d \cdot f \cdot (V - E_{\text{si}}) \tag{1.15}$$

$$E_{\text{si}} = 7.7 - 13.0287 \cdot \ln([\text{Ca}]_i) \tag{1.16}$$

Activation gate, d

$$
\begin{aligned}
\frac{dd}{dt} &= \alpha_d(1-d) - \beta_d d && (1.17a) \\
\alpha_d &= \frac{0.095e^{-0.01(V-5)}}{1+e^{-0.072(V-5)}} && (1.17b) \\
\beta_d &= \frac{0.07e^{-0.017(V+44)}}{1+e^{0.05(V+44)}} && (1.17c)
\end{aligned}
$$

Inactivation gate, f

$$
\begin{aligned}
\frac{df}{dt} &= \alpha_f(1-f) - \beta_f f && (1.18a) \\
\alpha_f &= \frac{0.012e^{-0.008(V+28)}}{1+e^{0.15(V+28)}} && (1.18b) \\
\beta_f &= \frac{0.0065e^{-0.02(V+30)}}{1+e^{-0.2(V+30)}} && (1.18c)
\end{aligned}
$$

Calcium uptake

$$\frac{d\left([\mathrm{Ca}]_i\right)}{dt} = -10^{-4} I_{\mathrm{si}} + 0.07(10^{-4} - [\mathrm{Ca}]_i) \qquad (1.19)$$

Outward Currents

Time-dependent potassium current

$$
\begin{aligned}
I_{\mathrm{K}} &= \overline{G}_{\mathrm{K}} \cdot X \cdot X_{\mathrm{i}} \cdot (V - E_{\mathrm{K}}) && (1.20) \\
\overline{G}_{\mathrm{K}} &= 0.282 \cdot \sqrt{[\mathrm{K}]_o/5.4} && (1.21)
\end{aligned}
$$

Activation gate, X

$$
\begin{aligned}
\frac{dX}{dt} &= \alpha_X(1-X) - \beta_X X && (1.22a) \\
\alpha_X &= \frac{0.0005e^{0.083(V+50)}}{1+e^{0.057(V+50)}} && (1.22b) \\
\beta_X &= \frac{0.0013e^{-0.06(V+20)}}{1+e^{-0.04(V+20)}} && (1.22c)
\end{aligned}
$$

Inactivation gate, X_{i}

$$X_{\mathrm{i}} = \begin{cases} \dfrac{2.837(e^{0.04(V+77)} - 1)}{(V+77)e^{0.04(V+35)}} & V > -100\mathrm{mV} \\ \\ 1 & V \leq -100\mathrm{mV} \end{cases} \tag{1.23}$$

Time-independent potassium current

$$I_{\mathrm{K1}} = \overline{G}_{\mathrm{K1}} \cdot \mathrm{K1}_{\infty} \cdot (V - E_{\mathrm{K1}}) \tag{1.24}$$

$$\overline{G}_{\mathrm{K1}} = 0.6047 \cdot \sqrt{[\mathrm{K}]_o/5.4} \tag{1.25}$$

Inactivation gate, K1

$$\mathrm{K1}_{\infty} = \frac{\alpha_{\mathrm{K1}}}{\alpha_{\mathrm{K1}} + \beta_{\mathrm{K1}}} \tag{1.26a}$$

$$\alpha_{\mathrm{K1}} = \frac{1.02}{1 + e^{0.2385(V - E_{\mathrm{K1}} - 59.215)}} \tag{1.26b}$$

$$\beta_{\mathrm{K1}} = \frac{0.49124e^{0.08032(V - E_{\mathrm{K1}} + 5.476)} + e^{0.06175(V - E_{\mathrm{K1}} - 594.31)}}{1 + e^{-0.5143(V - E_{\mathrm{K1}} + 4.753)}} \tag{1.26c}$$

Plateau potassium current

$$I_{\mathrm{Kp}} = \overline{G}_{\mathrm{KP}} \cdot \mathrm{Kp} \cdot (V - E_{\mathrm{Kp}}) \tag{1.27}$$

$$E_{\mathrm{Kp}} = E_{\mathrm{K1}} \tag{1.28}$$

$$\mathrm{Kp} = \frac{1}{1 + e^{(7.488 - V)/5.98}} \tag{1.29}$$

Background potassium current

$$I_{\mathrm{b}} = \overline{G}_{\mathrm{b}} \cdot (V - E_{\mathrm{b}}) \tag{1.30}$$

Total ionic current

$$
\begin{aligned}
I_{\mathrm{ion}} &= I_{\mathrm{Na}} + I_{\mathrm{si}} + I_{\mathrm{K}} + I_{\mathrm{K1}} + I_{\mathrm{Kp}} + I_{\mathrm{b}} \\
&= \overline{G}_{\mathrm{Na}} \cdot m^3 \cdot h \cdot j \cdot (V - E_{\mathrm{Na}}) + \overline{G}_{\mathrm{si}} \cdot d \cdot f \cdot (V - E_{\mathrm{si}}) \\
&\quad + \overline{G}_{\mathrm{K}} \cdot X \cdot X_{\mathrm{i}} \cdot (V - E_{\mathrm{K}}) + \overline{G}_{\mathrm{K1}} \cdot \mathrm{K1}_{\mathrm{inf}} \cdot (V - E_{\mathrm{K1}}) \\
&\quad + \overline{G}_{\mathrm{KP}} \cdot \mathrm{Kp} \cdot (V - E_{\mathrm{Kp}}) + \overline{G}_{\mathrm{b}} \cdot (V - E_{\mathrm{b}}) \qquad (1.31)
\end{aligned}
$$

1.4.3 The PDE model

The Luo-Rudy model describes the electrical activity of individual cells but not the propagation of impulses through the heart; in order to model this, the Luo-Rudy ODEs are combined with a parabolic partial differential equation,

$$
\begin{array}{lccc}
PDE: & c_m \frac{\partial V_m}{\partial t} & = & \nabla \cdot \mathbf{D}_r \nabla V_m - i_{ion}(V_m, t) + i_{app}(t) \\
BC: & \frac{\partial V_m}{\partial \mathbf{n}} & = & 0 \\
IC: & V_m(x, y, 0) & = & V_{rest}
\end{array} \qquad (1.32)
$$

This partial differential equation incorporates the Luo-Rudy ODEs in the i_{ion} term and accounts for the anisotropic electrical conductivities and shape of the muscle fibres with the conductivity matrix $\mathbf{D}_r$. $\mathbf{n}$ is the unit outward normal vector on the boundary. The Neumann boundary condition for the region models the condition that no current flows across the boundary. The initial condition we take is that the membrane potential be initially at its resting value. The PDE will be solved on a ventricular region H, an annulus representing a cross-section through the ventricle with external radius 5cm and internal radius 4cm. In terms of the x and y coordinates of the points in H, the conductivity matrix $\mathbf{D}_r$ is as follows,

$$\mathbf{D}_r = \begin{pmatrix} \sigma_l - \frac{x^2}{x^2+y^2}(\sigma_l - \sigma_t) & \frac{-xy}{x^2+y^2}(\sigma_l - \sigma_t) \\ \frac{-xy}{x^2+y^2}(\sigma_l - \sigma_t) & \sigma_t + \frac{x^2}{x^2+y^2}(\sigma_l - \sigma_t) \end{pmatrix}, \tag{1.33}$$

where σ_l is the longitudinal conductivity and σ_t is the transverse conductivity. H is an *anisotropic biodomain region* containing both intercellular and extracellular areas. Electrical conductivities in H are also anisotropic: in directions perpendicular to the fibre axis the conductivity is uniform but it differs in directions parallel to the axis. An important assumption is made concerning this anisotropy, namely that of equal conductivity ratios. The assumption is made for ease of analysis and computation [3]. There is evidence that the equal anisotropy assumption is not physiologically valid [5]; an interesting and important extension of this project would be to investigate the assumption using more sophisticated numerical methods to handle three-dimensional geometries; this extension is discussed further in Chapter 4.

Chapter 2

Solution Scheme and Numerical Methods

The PDE was solved on the annular region H using Matlab's PDE Toolbox. This Toolbox uses the *finite element method* to solve PDEs. There are three main advantages to using the Toolbox software for our simulations. The first is that because it is based on the finite element method we are able to solve our problem on an annular domain. Previous simulations by [3], [11], and [4] using finite differences have only been on less-realistic rectangular domains. In this respect, the investigation presented in this thesis is new. Secondly, using a commercially proven software package implementing the finite element method has its benefits. It makes the burden of writing our own software unnecessary and moreover it has already been optimized in terms of memory allocations for matrix storage, linear system solution, and time-stepping algorithms. Finally, Matlab has an excellent suite of graphics programs that allow us to visualize and interpret our results easily.

A disadvantage of this particular toolbox, however, is that it is restricted to solving problems in at most two dimensions. Strictly speaking, it is also not designed to solve a PDE coupled to ODEs. This is another feature of this work. Further investigations in the three-dimensional geometries will require the use of a more powerful software package such as FEMLAB. However, the experience gained from working with this model in two dimensions should make the transition to three dimensions a little smoother. The simulations in three dimensions are a topic for future investigation.

We now give a brief overview of the finite element method.

2.1 The Finite Element Method

The finite element method (FEM) approximates the solution to the PDE on a approximation of the domain composed of a mesh of elements whose vertices are called *nodes*. Matlab's PDE Toolbox uses linear basis functions on triangular meshes [9]. The approximation $U(x,y)$ to the solution $u(x,y)$ is a linear combination of test functions $T(x,y)$,

$$U(x,y) \approx \sum_{j=1}^{n} U_j T_j(x,y) \tag{2.1}$$

where U_i are scalar coefficients and n is large. The T_j are chosen so that they have a height 1 at node j and height 0 at all other nodes. The test functions must also satisfy the boundary conditions. The approximate solution u_h is tested against all test functions. For example, using Poisson's equation in two dimensions, $\nabla^2 u = f(x,y)$, this means that u_h is determined such that

$$\iint_R \nabla^2 u T_i dA = \iint_R f T_i dA, \qquad dA = dxdy. \tag{2.2}$$

When the left-hand side of the equation is integrated by parts using $\nabla \cdot (T_i \nabla u) = T_i \nabla^2 u + \nabla T_i \cdot \nabla u$, the result is

$$\iint_R [\nabla \cdot (T_i \nabla u) - \nabla T_i \cdot \nabla] dA = \iint_R f T_i dA. \tag{2.3}$$

and using the two-dimensional divergence theorem gives the *weak form* of the PDE which all solutions $u(x,y)$ must satisfy,

$$\iint_R \nabla T_i \cdot \nabla u dA = -\iint_R f T_i dA. \tag{2.4}$$

The approximate solutions $U(x,y)$ must satisfy the weak form,

$$\sum_{j=1}^{n} U_j \iint_R \nabla T_i \cdot \nabla T_j dA = -\iint_R f T_i dA \tag{2.5}$$

which gives the n equations for the the n unknown coefficients U_i, the values of $u(x,y)$ at the nodes. To solve for the coefficients a linear system $KU = F$ must be found. K is a stiffness matrix with entries $K_{ij} = K_{ji}$, where

$$K_{ij} = \iint_R \nabla T_i \cdot \nabla T_j dA. \tag{2.6}$$

The vector $\mathbf{F}$ has entries F_i,

$$F_i = -\iint_R f T_i dA \tag{2.7}$$

This gives n equations

$$\sum_{j=1}^{n} K_{ij} U_j = F_j \tag{2.8}$$

which are written in matrix form as $KU = F$ with formal solution $U = K^{-1}F$ [6]. The inverse of K is generally not computed in order to solve for U. Instead, LU decomposition of K is performed; this method requires fewer operations than calculating the inverse.

Chapter 3

Results and Simulations

The results in this chapter are presented in two parts: the solutions to the Luo-Rudy ODEs and the solution to the coupled system of the ODEs and the PDE given by (1.32). Although the simulation is for the propagation of action potentials in the domain H, it is relevant to see the solutions to the Luo-Rudy ODEs for action potentials generation in isolated cells. Thus, these solutions are presented as the first step in the simulation. The second part of the results gives the final simulation of the propagation of the action potentials that is the solution to (1.32).

3.1 Solving the Luo-Rudy ODEs

Before attempting to solve the full PDE problem for the propagation of the electrical activity, the i_{ion} term had to be computed; that is the Luo-Rudy ODEs had to be solved. There are eight equations in total: six for the gating parameters m, h, j, d, f, X, one for the calcium concentration Ca, and one for the membrane potential V_m. The parameters m (1.12), h (1.13), and j (1.14) are the activation, fast inactivation, and slow inactivation gates, respectively, of the fast inward sodium current I_{Na} (1.11). d (1.17) is the activation gate of the slow inward calcium current I_{si} (1.15), f (1.18) is its inactivation gate. This current is also dependent on the calcium uptake which is described with the ODE for internal calcium concentration (1.19). Of the outward currents, only the time-dependent potassium current (1.20) is associated with a gating parameter. X (1.22) is the activation gate of the time-dependent potassium current. The inactivation parameter, X_i (1.23), for this current is time-independent. The other three outward currents, the time-independent potassium (1.24), plateau potassium (1.27), and background potassium (1.30) currents, are time independent and thus can be calculated without the solution of ODEs. The time-independent potassium current does have an inactivation gate, $K1$, but its value is approximated by the steady state, $K1_\infty$ (1.26).

Before incorporating the PDE, a routine was written in Matlab to solve these eight ODEs and the resulting ionic currents on the annular region H. Table 3.1 shows the values of the channel conductances, the reversal potentials for the ions and other parameters. Plots of all the currents, time-dependent and independent, were

Table 3.1: Parameters for the Luo-Rudy Phase I model; the conductances are in mS/cm^2 and the reversal potentials in mV [3].

Channel Conductance	Reversal Potential	Other Parameters
$\overline{G}_{\mathrm{Na}} = 23.0$	$E_{Na} = 54.4$	Resting Membrane Potential V_{rest} = -84.0mV
$\overline{G}_{\mathrm{si}} = 0.09$	$E_{si} = 118.7$	Membrane Threshold Potential $V_{threshold}$ = -60mV
$\overline{G}_{\mathrm{K}} = 0.282$	E_K = -77	Intracellular Calcium
$\overline{G}_{\mathrm{K1}} = 0.6047$	E_{K1} = -87.2	Concentration $[Ca]_i = 2.0 \times 10^{-4}$ mM
$\overline{G}_{\mathrm{Kp}}$ = 0..0183	E_{Kp} = -87.2	
$\overline{G}_{\mathrm{b}} = 0.03921$	E_b = -59.87	

generated along with plots for the calcium concentration and the membrane potential. All plots were constructed over a 450ms time frame and are shown in Figures 3.1–3.8. Because of the stiff nature of the LR ODEs, the solutions were obtained using the Matlab solver ode15s. This solver is an implicit, multistep method based on so-called numerical differentiation formulas of varying order (1-5). The solver ode15s was able to accommodate the rapid changes in the solution by taking small time steps as required. The solver ode45, an explicit Runge-Kutta medium-order (4-5) solver, was tried but the numerical solution became unstable. The solutions to the Luo-Rudy ODEs and the corresponding ionic currents agree with those found by Clements [3].

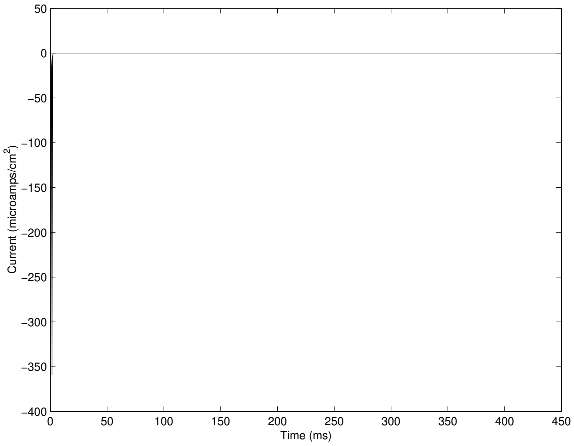

Figure 3.1: Fast inward sodium current over the duration of the action potential.

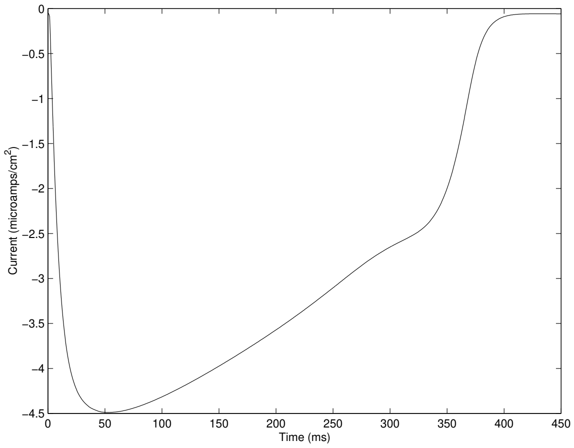

Figure 3.2: Slow inward (calcium) current over the duration of the action potential.

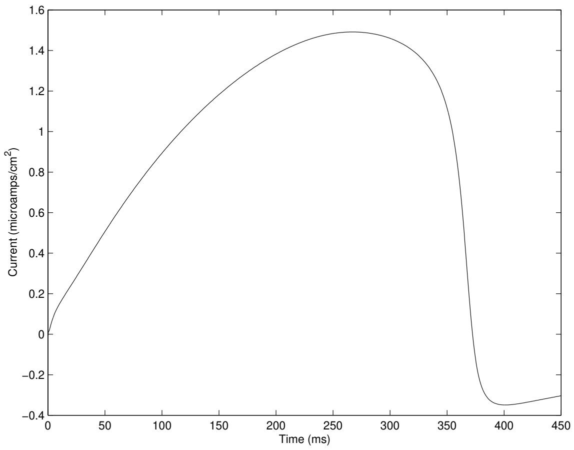

Figure 3.3: Time-dependent potassium current over the duration of the action potential.

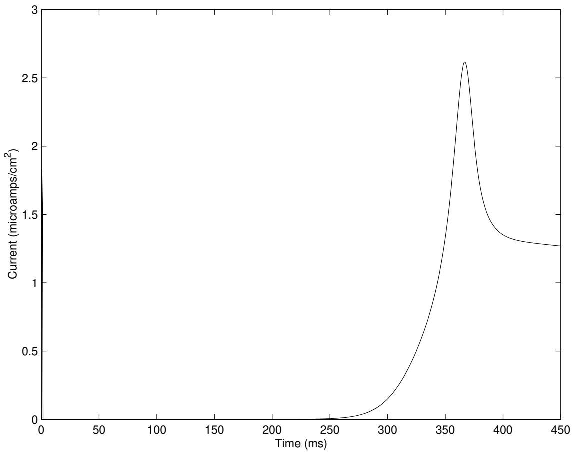

Figure 3.4: Time-independent potassium current over the duration of the action potential.

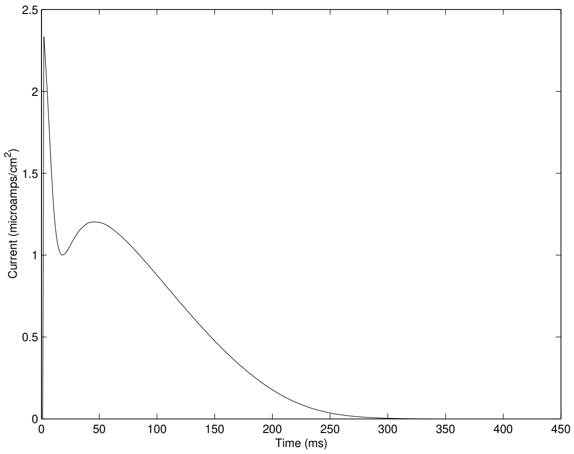

Figure 3.5: Plateau potassium current over the duration of the action potential.

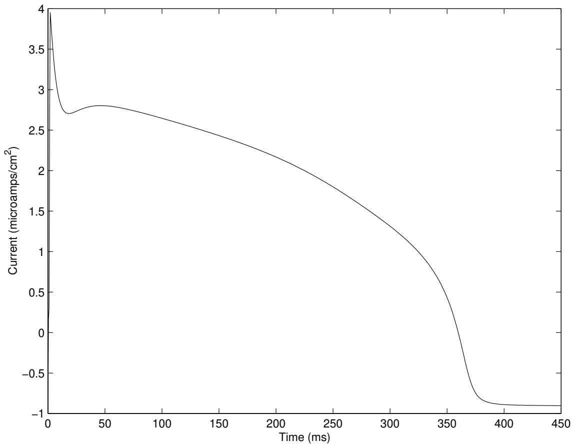

Figure 3.6: Background potassium current over the duration of the action potential.

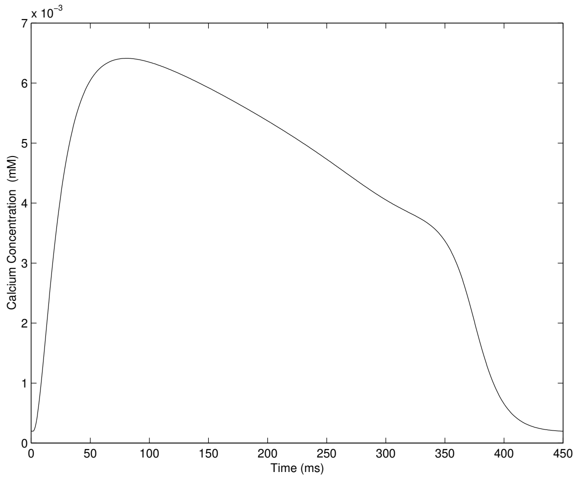

Figure 3.7: Intracellular calcium concentration over the duration of the action potential.

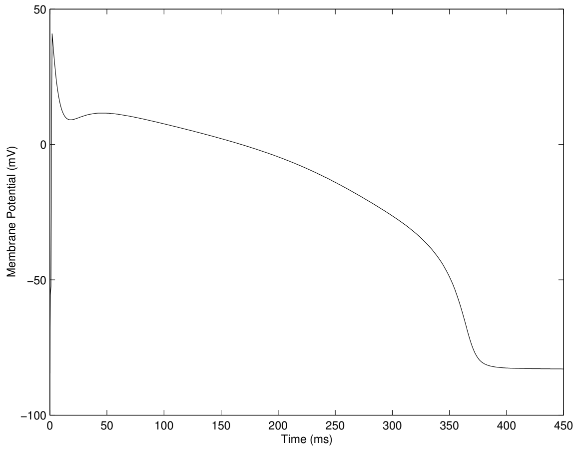

Figure 3.8: Membrane potential over the duration of the action potential.

3.2 Solving the PDE

Once the solutions to the Luo-Rudy ODEs were obtained and the corresponding ionic currents calculated, the next step was to incorporate these results into the PDE recalled below,

$$\begin{array}{llcc} PDE: & c_m \frac{\partial V_m}{\partial t} & = & \nabla \cdot \mathbf{D}_r \nabla V_m - i_{ion}(V_m, t) + i_{app}(t) \\ BC: & \frac{\partial V_m}{\partial \mathbf{n}} & = & 0 \\ IC: & V_m(x, y, 0) & = & V_{rest} \end{array}$$

and obtain a solution in the annular region H. Figure 3.9 shows the triangular mesh on H. The mesh consists of 87 nodes at which the solution to the PDE was approximated using Matlab's PDE Toolbox. While the annulus and mesh were created using the Graphical User Interface, all the components of the PDE could not be entered using this interface. The coupling of the Luo-Rudy ODEs and the conductivity matrix D_r made it necessary to export the mesh to the workspace and write a routine to solve the PDE. Some of the parameter values for the PDE are shown in Table 3.2.

Table 3.2: Parameter values for the PDE.

Equal anisotropy ratio r	4
Transverse conductivity σ_t	0.5 mS/cm
Longitudinal conductivity σ_l	2.0 mS/cm
Membrane Capacitance C_m	1 μF/cm^2
Surface to volume ratio χ	200 cm^{-1}

The solution illustrates the propagation of the action potentials around the annulus. The stimulus current I_{app} was applied at node 8 (point $(4, 0)$) on the far right of the annulus and the wave successfully passed across the entire region. For a single point stimulus the required applied current to trigger an action potential was 8250 μA/cm for 0.25ms. A line stimulus over five nodes was also performed and found to trigger action potential propagation with an applied current of 1850 μA/cm for 0.25ms. A plot of the membrane potential versus time at the node to which the stimulus was applied is shown in Figure 3.9. The action potentials at all other nodes are identical in size and shape but are offset slightly in time according to their position in the annular region. A Matlab movie showing the the spread of the wave of electrical activity around the annulus was also produced.

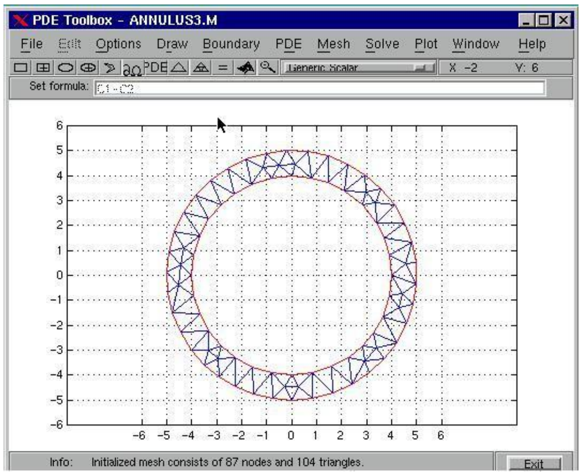

Figure 3.9: The 87 point triangular mesh on the domain H

Chapter 4

Conclusions and Future Work

We were successful in simulating the propagation of action potential in ventricular muscle with our model. The 2-D annular domain H was more physiologically accurate than the sheet or rectangular domains normally used, as in [11] and [3]. The conductivity matrix D_r accounted for the shape of the muscle fibres as well as the anisotropy in their conduction. Furthermore, the Luo-Rudy Phase I model accounts for more of the ionic currents than the commonly used Beeler-Reuter membrane model. The combination of annular domain and the Luo-Rudy model make the work presented in this thesis new.

There are many options for further investigation. The following are a few of the possibilities, including both further simulations with the existing model as well as improvements to it:

- Investigation of reentrant activity
- Incorporation of Luo-Rudy Phase II model
- Simulations without an assumption of equal anisotropy ratio
- Simulations in three dimensional domains

The existing model can be used to study the conditions under which reentrant activity can be incited in cardiac muscle. Reentrant electrical activity results from the premature stimulation of previously excited tissue. As the wave of excitation passes through the muscle it leaves behind it cells which have fired an are, for a certain length of time, unable to be re-excited. This period of non-excitability is known as the *refractory period*. Cardiac muscle cells have a longer refractory period than other muscle cells. This is marked by a longer plateau phase of the action potential. The refractory period protects against the rapid uncoordinated contraction that can result from successive premature stimuli. In order for reentrant activity to propagate, the premature stimulus must occur at a location and time such that the it is able to excite the cells in the wake of the original wave of excitation but not those lying ahead of it in the path of the wave. This re-stimulation of only part of the muscle is believed to be the underlying cause of tachycardia (rapid heart rate) and fibrillation (rapid, uncoordinated contraction) [4]. Therefore this investigation has important clinical applications.

Improvements to the model to increase the physiological accuracy can be made. Use of the Luo-Rudy Phase II model would give a more detailed description of the ionic activity in ventricular muscle cells by incorporating more of the processes that that occur at the molecular level in the cells, including the action of ionic pumps and changes in ionic concentrations. This model has many more parameters than the Phase I model and its use would increase computational difficulty. The assumption of the equal anisotropy ration is also a simplification to ease computation. Removal of this assumption, which there is evidence against [5], would also improve the accuracy but at the expense of the difficulty in numerical calculations. Finally, a move to a three dimensional domain which retains at least all the accuracy of the existing two dimensional one would be a logical progression. More powerful software such as FEMLAB would be needed to compute solutions on such a domain.

Bibliography

[1] Dalya Abdulla, *An Integral Formulation for the Solution of a Nonlinear Wave-Propagation Problem*, Masters Thesis, Department of Mathematics and Statistics, Dalhousie University, 2000.

[2] Neil A. Campbell. *Biology, Fourth Edition.* Benjamin/Cummings Publishing Company, California, 1996.

[3] Clyde J. Clements, *Nonlinear Wave Propagation in an Anisotropic Medium*, Masters Thesis, Department of Mathematics, Statistics, and Computing Science, Dalhousie University, 1996.

[4] Clyde J. Clements, John C. Clements, and B. Milan Horacek, *On the formation of scroll waves in an anisotropic ventricular myocardium*, Fields Institute Communications, **21**, 97–106, 1991.

[5] John C. Clements, Department of Mathematics and Statistics, Dalhousie University, Personal Communication.

[6] Richard Haberman, *Elementary Applied Partial Differential Equations, Third Edition*, Prentice-Hall Inc., New Jersey, 1998.

[7] Ching-hsing Luo and Yoram Rudy, *A model of the ventricular cardiac action potential: Depolarization, repolarization, and their interaction*, Circ. Res., **68(6)**, 1501–1526, 1991.

[8] Elaine N. Marieb, *Essentials of Anatomy and Physiology, Sixth Edition*, Addison Wesley Longman, Inc., 2000.

[9] *Partial Differential Equation Toolbox User's Guide*, MathWorks, The MathWorks Inc., 1995.

[10] David Randall, Warren Burggren, and Kathleen French, *Eckert Animal Physiology, Mechanisms and Adaptations, Fourth Edition*, W. H. Freeman and Company, New York, 1997.

[11] F. A. Roberge, A. Vinet, and B. Victorri, *Reconstruction of Propagated Electrical Activity with a Two-Dimensional Model of Anisotropic Heart Muscle*, Circ. Res., **58**, 461–475, 1986.